Journal of Nanobiotechnology

RESEARCH

Open Access

Coptis chinensis-derived extracellular vesicle-like nanoparticles delivered miRNA-5106 suppresses NETs by restoring zinc homeostasis to alleviate colitis

Yi Yang[1,2,3†], Lanmengxi Yang[1,2,3†], Haiyi Deng[1,2,3], Yuheng Liu[1,2,3], Junwei Wu[1,2,3], Yilin Yang[1,2,3], Jin Su[1,2,3], Shiyu Su[1,2,3], Junhao Xu[1,2,3], Jie Wei[4], Xiaoyan Deng[1,2,3], Yujin Wu[1], Yao Liao[1,2,3*] and Lifu Wang[1,2,3*]

Abstract

Background Inflammatory bowel disease (IBD) is a chronic disorder marked by persistent inflammation and damage to the intestinal mucosa. Despite significant advances in treatment, there remains an unmet need for more effective and safer therapeutic strategies.

Results In this study, we isolated and characterized extracellular vesicle-like nanoparticles (ELNs) derived from *Coptis chinensis* (Cc-ELNs) and evaluated their therapeutic potential in IBD. Intraperitoneal administration of Cc-ELNs in dextran sulfate sodium (DSS)-induced colitis mice demonstrated selective targeting of inflamed intestinal regions. Cc-ELNs significantly alleviated colitis by reducing neutrophil recruitment and inhibiting the formation of neutrophil extracellular traps (NETs). Furthermore, by suppressing NET formation, Cc-ELNs mitigated pyroptosis in intestinal epithelial cells (IECs) and promoted the proliferation of both IECs and intestinal stem cells (ISCs). Mechanistically, Cc-ELNs delivered miR-5106, which downregulated *Slc39a2* expression, thereby restoring zinc homeostasis in neutrophils and reducing NET formation.

Conclusions These findings establish Cc-ELNs as a novel, natural, and effective therapeutic candidate for IBD, highlighting the potential of plant-derived nanoparticle-based therapies.

Keywords Inflammatory bowel disease, *Coptis chinensis*, Extracellular vesicle-like nanoparticles, Neutrophil, Neutrophil extracellular trap

†Yi Yang and Lanmengxi Yang contributed equally to this work.

*Correspondence:
Yao Liao
2023390084@gzhmu.edu.cn
Lifu Wang
wanglf@gzhmu.edu.cn

Full list of author information is available at the end of the article

Graphical Abstract

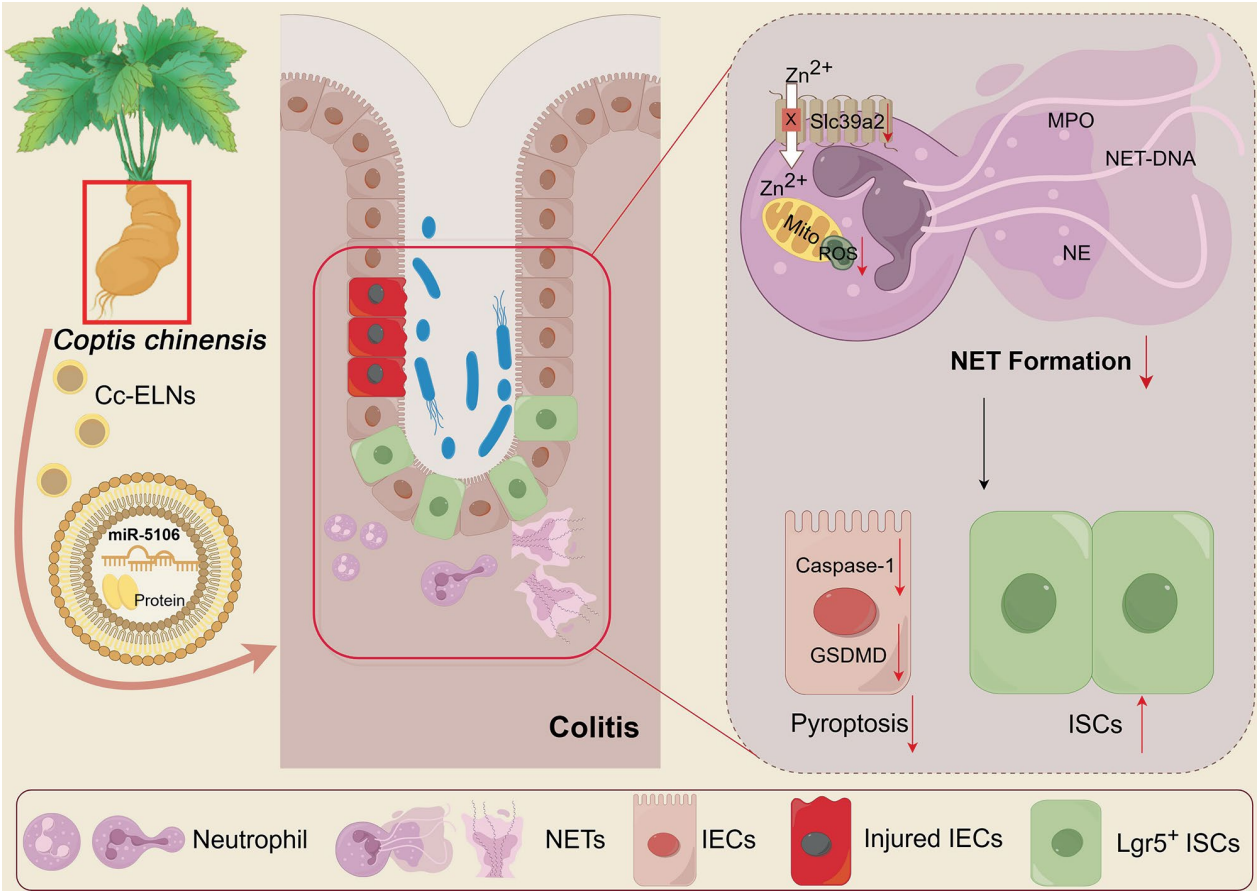

Introduction

Inflammatory bowel disease (IBD), encompassing Crohn's disease and ulcerative colitis, has seen a notable rise in global prevalence over the past decade [1]. It is characterized by chronic damage to the colonic epithelial mucosa, leading to a relapsing and remitting disease course [2]. Although its precise etiology remains elusive, IBD is widely believed to result from an aberrant immune response to intestinal microbiota in genetically predisposed individuals [3]. A hallmark feature of IBD is dysregulated intestinal immune activity, including the accumulation of neutrophils in inflamed mucosa, which plays a critical role in disease progression [4]. Neutrophils, the most abundant white blood cells and first responders to inflammation, are short-lived effector cells of the innate immune system [5, 6]. Recent studies underscore the importance of neutrophil extracellular traps (NETs), web-like structures released by activated neutrophils, in driving systemic autoimmune disorders and exacerbating inflammation-associated tissue damage [7]. Elevated NET formation has been observed in both IBD patients and DSS-induced colitis models [8, 9].

Extracellular vesicles (EVs), nanoscale biological carriers of bioactive molecules, are emerging as promising tools for intercellular communication and therapeutic applications [10]. EVs have demonstrated safety and efficacy in preclinical models and early clinical trials [11, 12]. Recently, extracellular vesicle-like nanoparticles (ELNs) derived from edible plants (P-ELNs) have gained attention for their potential in inter-kingdom delivery of therapeutic payloads, including nucleic acids [13–17]. P-ELNs from ginger, lemon, grapefruit, grapes, and *Portulaca oleracea L.* have shown efficacy in treating colitis [18–21], while P-ELNs from plants such as ginseng and *Asparagus cochinchinensis* have exhibited anticancer properties [22, 23]. Additionally, P-ELNs have demonstrated therapeutic potential in conditions such as alcoholic hepatitis and infectious diseases [13]. P-ELNs offer several advantages, including biocompatibility, biodegradability, low immunogenicity, and scalability, positioning them as highly promising platforms for drug delivery.

Traditional Chinese medicine has long utilized *Coptis chinensis* (Huanglian) for treating gastrointestinal disorders, including ulcers and inflammation [24]. Extensive

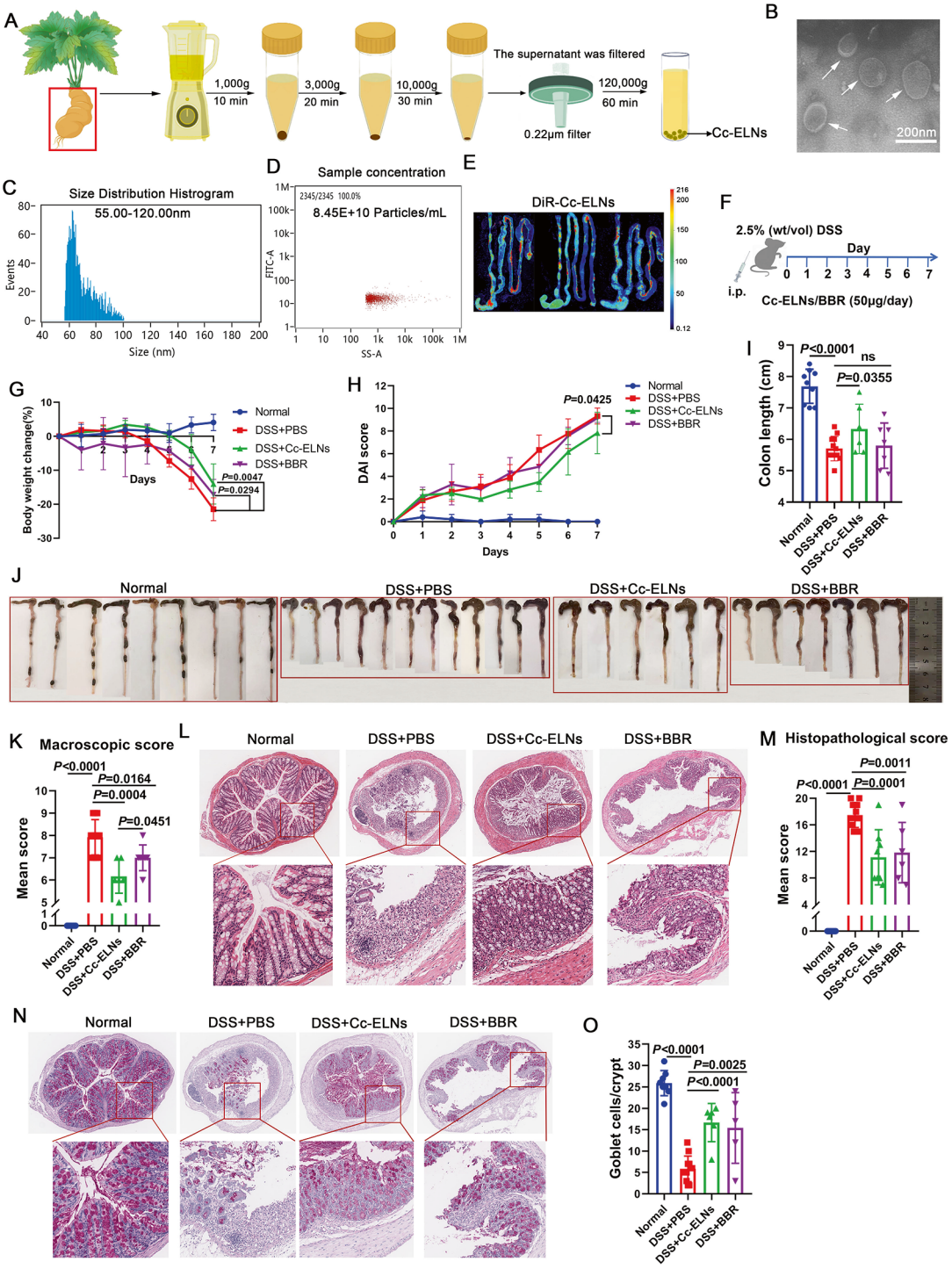

Fig. 1 (See legend on next page.)

research has identified its pharmacological properties, which include hypoglycemic, antibacterial, antioxidant, anti-inflammatory, antitumor, lipid-regulating, and anti-arrhythmic effects [24]. Study has found that *Coptis chinensis* might prevent intestinal barrier damage in TNBS-induced ulcerative colitis by inhibiting the inflammatory response [24]. The mixture of *Anemarrhena asphodeloides* and *Coptis chinensis* has been shown to attenuate high-fat diet-induced colitis in mice [25]. Furthermore, *Coptis chinensis* alleviates dextran sodium sulfate (DSS)-induced colitis in mice [26]. Additionally, berberine (BBR), the active component of *Coptis chinensis*, has demonstrated protective effects in colitis models [27–29].

(See figure on previous page.)

Fig. 1 Isolation and characterization of extracellular vesicle-like nanoparticles (Cc-ELNs) derived from *Coptis chinensis* and their protective effect against DSS-induced colitis in mice. (**A**) Cc-ELNs were isolated from fresh *Coptis chinensis* juice through a multi-step differential centrifugation process. (**B**) Transmission electron microscopy (TEM) image showing the cup-shaped morphology of Cc-ELNs. (**C**, **D**) Nanoflow cytometry analysis was used to determine the size distribution (**C**) and concentration (**D**) of Cc-ELNs. (**E**) DiR-labeled Cc-ELNs were injected intraperitoneally into mice, and their distribution was observed in the intestinal tissues (jejunum, ileum, cecum, and colon) after 24 h post-injection. (**F**) Mice with DSS-induced colitis were treated with intraperitoneal injections of Cc-ELNs, with berberine (BBR) serving as a positive control. (**G**) Time course of body weight changes in the experimental groups, normalized to Day 0 body weight. (**H**) Disease Activity Index (DAI) scores based on symptoms such as diarrhea, bleeding, and body weight loss. (**I**) Measurement of colon length from mice in different treatment groups. (**J**) Macroscopic appearance of the colon, as represented by a colon with mean colon length and typical injury findings. (**K**) Macroscopic colon scores indicating the severity of colon injury. (**L**) Histopathological examination of colon tissues stained with H&E. (**M**) Histopathological scores for the colon tissue samples determined through H&E staining. (**N**, **O**) Alcian blue-periodic acid-Schiff (AB-PAS) staining to detect goblet cell depletion (**N**), with goblet cell counts presented (**O**). $n = 5–12$; Statistical significance was determined using one-way ANOVA followed by Tukey's multiple comparison test

Zinc is an essential element that plays a vital role in various biological processes, functioning as a structural, catalytic, and signaling component [30]. Zinc homeostasis is regulated by transporters, including the ZIP (Slc39) and ZnT (Slc30) families, with dysregulation of these transporters linked to the onset and progression of numerous diseases [30, 31].

In this study, we isolated and characterized *Coptis chinensis*-derived ELNs (Cc-ELNs) for the first time. Our results demonstrated that intraperitoneal injection of Cc-ELNs specifically targeted inflamed sites in DSS-induced colitis mice. Additionally, Cc-ELNs significantly alleviated colitis by reducing neutrophil recruitment and inhibiting NET formation. By inhibiting NETs, Cc-ELNs mitigated pyroptosis in intestinal epithelial cells (IECs) and promoted the proliferation of both IECs and intestinal stem cells (ISCs). Mechanistically, Cc-ELNs delivered miR-5106, which downregulated Slc39a2 expression, thereby restoring zinc homeostasis in neutrophils and reducing NET formation.

Results

Cc-ELNs protect mice against DSS-induced colitis

Cc-ELNs were isolated from fresh *Coptis chinensis* juice using a multi-step differential centrifugation protocol (Fig. 1A). Transmission electron microscopy (TEM) revealed the characteristic cup-shaped morphology of Cc-ELNs (Fig. 1B), while nanoflow cytometry analysis indicated their size distribution ranged from 55 to 120 nm in diameter (Fig. 1C), with a concentration of approximately 8.45×10^{10} particles/mL (Fig. 1D). DiR-labeled Cc-ELNs were then intraperitoneally injected into mice, and 24 h later, their distribution in intestinal tissues was assessed. Cc-ELNs were found throughout the jejunum, ileum, cecum, and colon (Fig. 1E). To evaluate their therapeutic potential, mice with DSS-induced colitis were treated with intraperitoneal Cc-ELNs (Fig. 1F). BBR, a monomer derived from *Coptis chinensis*, has previously demonstrated protective effects in colitis models [27–29], and was used as a positive control at an equivalent dose to Cc-ELNs.

As shown in Fig. 1G, the DSS + Cc-ELNs group exhibited significantly less body weight loss from Day 4 compared to the DSS + PBS group, with a smaller trend of weight loss in the Cc-ELNs group than in the BBR group. The Disease Activity Index (DAI) of the DSS + Cc-ELNs group was consistently lower than the DSS + PBS group from Day 3 onward (Fig. 1H). DSS treatment resulted in substantial colon shortening in colitis mice (Fig. 1I, J), but the DSS + Cc-ELNs group displayed significantly longer colon lengths compared to the DSS + PBS group (Fig. 1I, J). Similarly, the macroscopic colon scores in the DSS + Cc-ELNs group were significantly lower than those in the DSS + PBS group (Fig. 1K). Histological analysis showed that DSS caused major disruption of colonic architecture, with neutrophil and lymphohistiocyte infiltration, crypt loss, crypt abscess formation, submucosal edema, and goblet cell depletion. Treatment with Cc-ELNs significantly alleviated these structural disruptions compared to the DSS + PBS group (Fig. 1L). Histological scores were also markedly reduced in Cc-ELNs-treated mice (Fig. 1M), and goblet cell depletion was notably alleviated (Fig. 1N, O). Across multiple measures, including body weight loss, colon length, and macroscopic colon scores, the therapeutic effects of Cc-ELNs outperformed those of BBR (Fig. 1G-O). These findings collectively suggest that Cc-ELNs provide significant protection against DSS-induced colitis in mice.

Cc-ELNs inhibit neutrophil recruitment in colitis mice

Neutrophil infiltration into the intestinal mucosa is a defining feature of active IBD [32]. To investigate whether the therapeutic effects of Cc-ELNs on colitis are linked to neutrophil regulation, we assessed neutrophil levels in both the intestinal mucosa and Peyer's patches. In DSS-induced colitis mice, substantial neutrophil infiltration was observed in both the intestinal mucosa and Peyer's patches, which was significantly reduced following treatment with Cc-ELNs and BBR (Fig. 2A, Figure S1A, B). Notably, neutrophil reduction was more pronounced in the Cc-ELNs-treated group than in the BBR group (Fig. 2A, Figure S1A, B). In addition to the intestinal tissues, DiR-labeled Cc-ELNs were also enriched in the

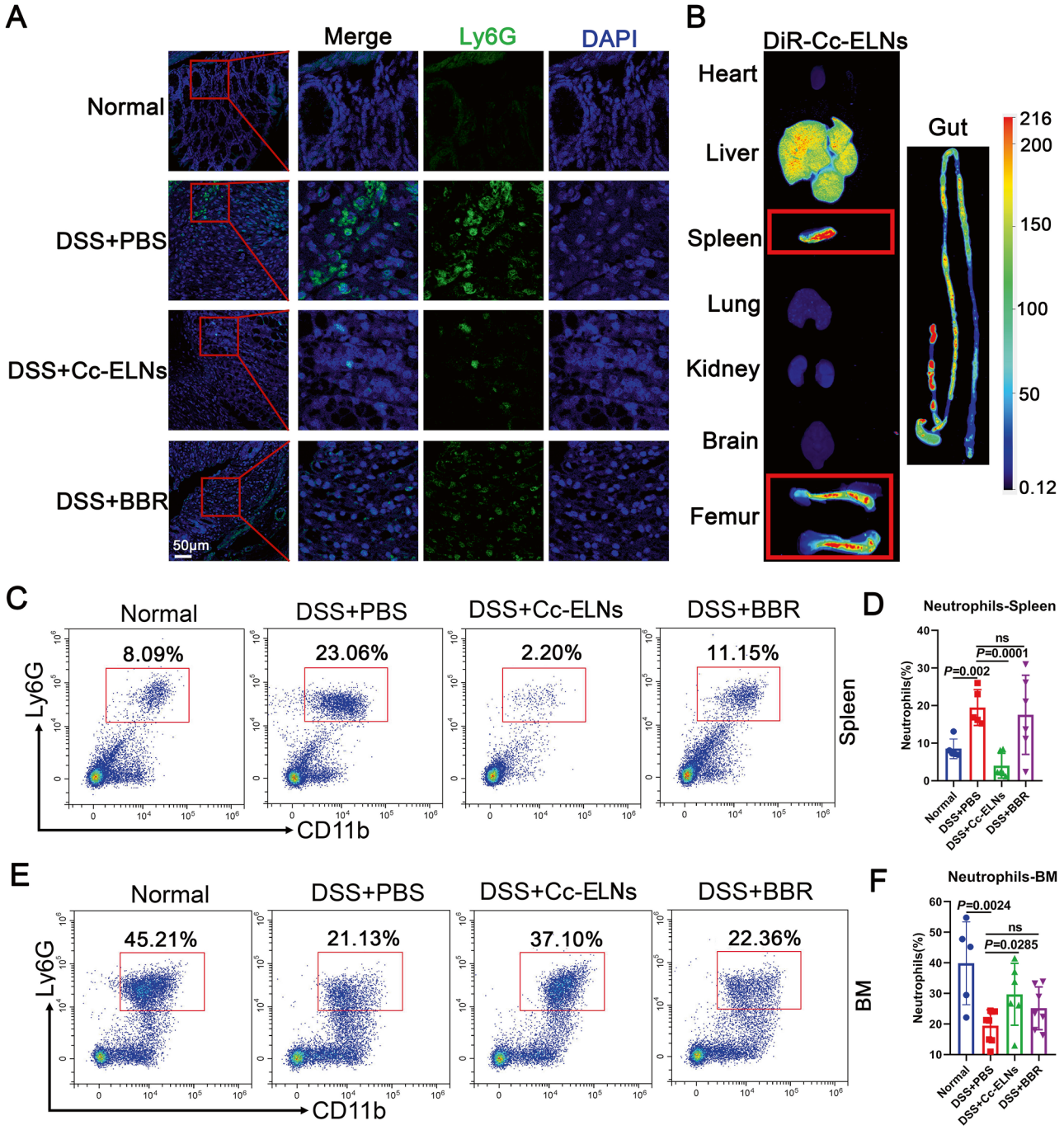

Fig. 2 Cc-ELNs inhibit neutrophil recruitment in DSS-induced mice. (**A**) Immunofluorescence analysis of neutrophil counts in the colon tissue of mice. (**B**) DiR-labeled Cc-ELNs were intraperitoneally injected into mice, and the biodistribution of Cc-ELNs was assessed in the femur, heart, liver, spleen, lungs, kidneys, brain, and gut using ex vivo imaging. (**C**–**F**) Percentages of neutrophil counts in the spleen and bone marrow (BM) were analyzed by flow cytometry (**C**, **E**), and the statistical analysis results are shown (**D**, **F**). $n = 5$–7; Statistical significance was determined using one-way ANOVA followed by Tukey's multiple comparison test

spleen and bone marrow (BM; Fig. 2B). To further assess neutrophil levels, we evaluated spleens and BM. Neutrophil levels in the spleens of Cc-ELNs-treated colitis mice were significantly lower than those in PBS-treated mice (Fig. 2C, D). Interestingly, BM neutrophil levels were markedly reduced in DSS-induced colitis mice compared to normal mice (Fig. 2E, F), likely due to the recruitment of neutrophils to peripheral organs during acute colitis. Cc-ELNs treatment alleviated this peripheral neutrophil recruitment, thereby restoring neutrophil levels in the BM (Fig. 2E, F).

Cc-ELNs inhibit NET formation in colitis mice

To explore whether Cc-ELNs affect neutrophil function beyond recruitment inhibition, we examined changes in neutrophil activity. Immunofluorescence analysis revealed a significant increase in NET formation in the intestinal mucosa of colitis mice, which was notably reduced following Cc-ELNs treatment (Fig. 3A). To determine whether this downregulation of NET formation was due solely to a decrease in neutrophil numbers or an inhibitory effect on neutrophil function, we cultured neutrophils isolated from the BM and spleens of mice in vitro. Neutrophils from colitis mice easily formed NETs in vitro, whereas NET formation was significantly reduced in neutrophils from Cc-ELNs-treated mice (Fig. 3B-D). Phorbol 12-myristate 13-acetate (PMA), a NET inducer, showed that neutrophils from PBS-treated colitis mice were more susceptible to PMA-induced NET formation in vitro compared to those from Cc-ELNs-treated colitis mice (Figure S2A-C). To investigate whether Cc-ELNs directly or indirectly inhibit NET formation, we isolated BM and spleen neutrophils from normal mice and treated them with Cc-ELNs, using PMA to induce NET formation in vitro. We observed that Cc-ELNs were internalized by neutrophils (Fig. 3E) and significantly inhibited PMA-induced NET formation (Fig. 3F-H). These findings suggest that Cc-ELNs directly inhibit NET formation in neutrophils from colitis mice.

Cc-ELNs alleviate intestinal epithelial injury by inhibiting NET formation

Intestinal epithelial damage is a key pathological feature of IBD. We observed significantly reduced cell proliferation in the intestinal mucosa of colitis mice compared to normal controls (Fig. 4A, Figure S3A). Cc-ELNs treatment significantly restored cell proliferation (Fig. 4A, Figure S3A). Pyroptosis, a form of programmed cell death triggered by inflammasome-mediated caspase-1 activation, is another critical process in IBD pathogenesis [33]. Gasdermin D (GSDMD) serves as a key executor in pyroptosis [34]. The expression levels of GSDMD and caspase-1 were elevated in the colons of colitis mice and were significantly reduced following Cc-ELNs treatment

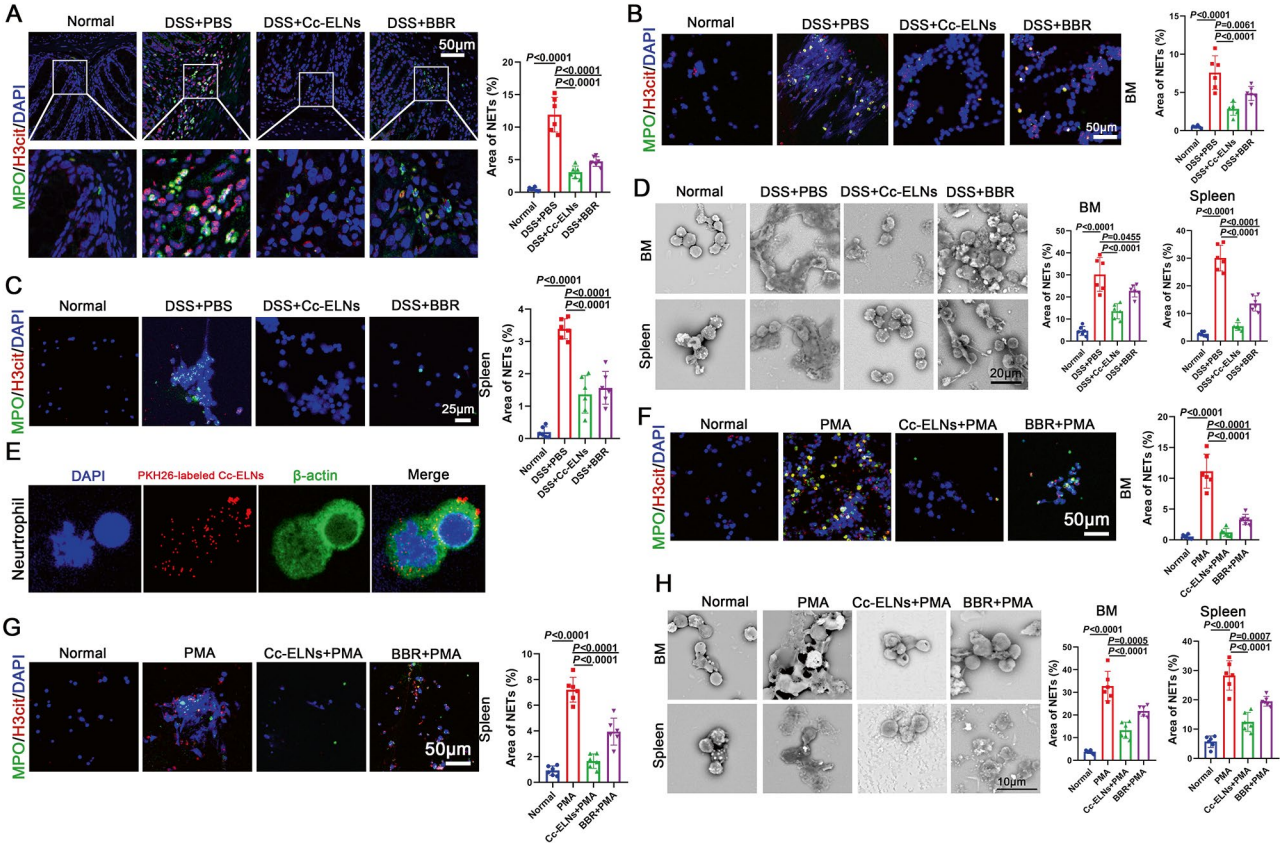

Fig. 3 Cc-ELNs inhibit NET formation in DSS-induced colitis mice. (**A**) Immunofluorescence analysis was used to evaluate NET formation in colon tissues. Co-localization of H3cit and MPO was used as a marker for NET detection. (**B**–**D**) Neutrophils isolated from the BM and spleen of mice were cultured in vitro for 24 h. Immunofluorescence analysis and scanning electron microscopy (SEM) were used to assess NET formation. (**E**) Neutrophils were incubated with PKH26-labeled Cc-ELNs, and internalization of Cc-ELNs was visualized through laser scanning confocal microscopy. (**F**–**H**) Neutrophils from BM and spleens of normal mice were treated with Cc-ELNs and BBR, followed by PMA-induced NET formation in vitro. NETs were assessed by immunofluorescence and SEM. $n = 6$; Statistical significance was determined using one-way ANOVA followed by Tukey's multiple comparison test

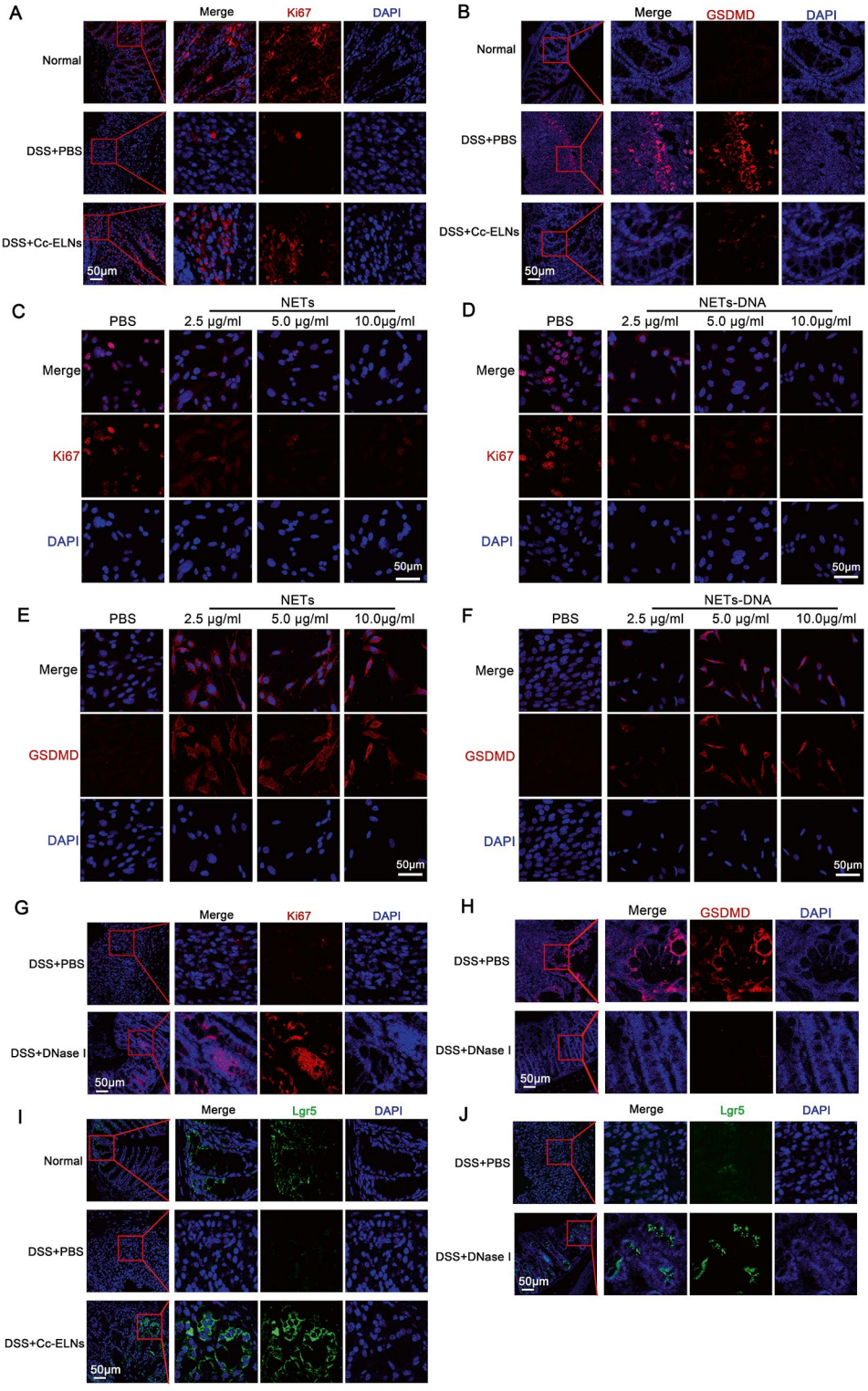

Fig. 4 Cc-ELNs alleviate intestinal epithelial injury by inhibiting NET formation. (**A**) Ki67 staining was performed on colon tissues to evaluate cell proliferation levels. (**B**) Immunofluorescence analysis was used to detect gasdermin D (GSDMD), a marker of pyroptosis, in the colon tissues. (**C**–**F**) Intestinal epithelial cells (IECs) were treated with NETs and NETs-derived DNA, and the levels of Ki67 and GSDMD were assessed by immunofluorescence analysis. (**G**, **H**) Colitis mice were treated with DNase I to inhibit colonic NET formation, and Ki67 and GSDMD expression levels in the colon tissue were evaluated. (**I**) $Lgr5^+$ cells in the intestinal mucosa were detected by immunofluorescence to assess intestinal stem cells (ISCs). (**J**) DNase I was used to inhibit colonic NET formation in colitis mice, and ISCs in the intestinal mucosa were detected using immunofluorescence analysis

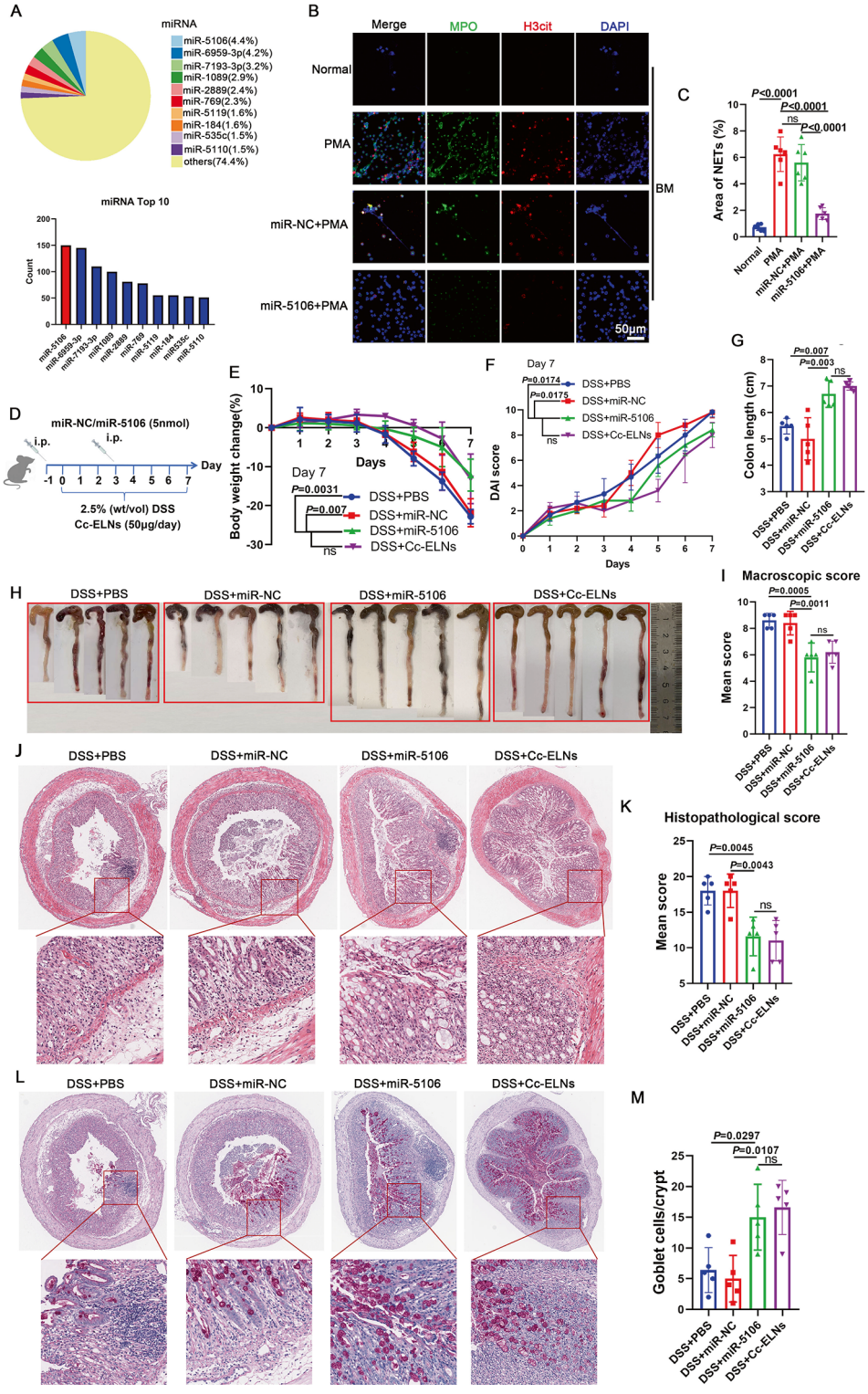

Fig. 5 (See legend on next page.)

(Fig. 4B, Figure S3B, C). To further investigate whether Cc-ELNs promote intestinal mucosal proliferation and inhibit pyroptosis by modulating NET formation, we stimulated intestinal epithelial cells (IECs) with extracted NETs. Interestingly, NETs (a DNA-protein complex) markedly inhibited IEC proliferation in a concentration-dependent manner (Fig. 4C, Figure S3D). NETs are composed of chromatin DNA filaments (NETs-DNA) coated

(See figure on previous page.)

Fig. 5 Cc-ELNs protect mice against DSS-induced colitis by delivering miR-5106 in high abundance. (**A**) Expression profile of miRNAs in Cc-ELNs was analyzed using small RNA sequencing, with the top 10 most highly expressed miRNAs presented. (**B**, **C**) Neutrophils treated with PMA and miR-5106 were analyzed for NET formation using immunofluorescence microscopy. (**D**) Mice with DSS-induced colitis were treated through intraperitoneal injection with miR-NC, miR-5106, or Cc-ELNs. (**E**) Body weight loss during the colitis progression was recorded, with Day 0 serving as the baseline (set at 0%). (**F**) Changes in the DAI were assessed. (**G**) On Day 7, mice were euthanized, and their colon tissues were excised and measured for length. (**H**) Macroscopic appearance of the colons was recorded. (**I**) Average macroscopic colon scores were calculated for each group. (**J**) Histopathological changes in colon tissues were examined using H&E staining. (**K**) Histopathological scoring was conducted for the colon tissue samples. (**L**, **M**) AB-PAS staining was used to assess goblet cell depletion in the colon (**L**), and quantification of goblet cells shown (**M**). $n = 5–6$; Statistical significance was determined using one-way ANOVA followed by Tukey's multiple comparison test

with granule proteins, and previous studies have shown that NETs-DNA is critical for the biological function of NETs [35]. We extracted NETs-DNA and stimulated IECs, observing that NETs-DNA significantly inhibited IEC proliferation in a concentration-dependent manner, as shown in Fig. 4D and Figure S3E. Additionally, both NETs and NETs-DNA upregulated GSDMD expression in IECs (Fig. 4E-F, Figure S3F-G). To investigate the role of NET formation in colitis, we inhibited colonic NET formation in mice using DNase I and assessed the expression levels of Ki67 and GSDMD in colonic tissue (Figure S4). Inhibition of NET formation resulted in an upregulation of Ki67 and a downregulation of GSDMD in the colon (Fig. 4G and H, Figure S5A and B). Intestinal epithelial renewal and patterning are regulated by ISCs [36]. In colitis mice, $Lgr5^+$ ISCs in the intestinal mucosa were significantly reduced compared to normal controls, but their levels were notably upregulated following Cc-ELNs treatment (Fig. 4I, Figure S6A). Similarly, ISC levels increased significantly after NET formation inhibition in colitis mice (Fig. 4J, Figure S6B).

These results suggest that Cc-ELNs alleviate intestinal epithelial injury in colitis mice by inhibiting pyroptosis and promoting ISC upregulation through NET formation inhibition.

Cc-ELNs protect mice against DSS-induced colitis by carrying miR-5106 in high abundance

MicroRNAs (miRNAs), key components of EVs, regulate gene expression [37]. We assessed the miRNA profile in Cc-ELNs and found miR-5106 to be the most highly expressed (Fig. 5A). We then explored miR-5106's role in Cc-ELNs-mediated NET inhibition. BM neutrophils treated with miR-5106 showed significantly reduced PMA-induced NET formation (Fig. 5B, C). To evaluate miR-5106's therapeutic effect, we administered miR-5106 to colitis mice via intraperitoneal injection (Fig. 5D). As shown in Fig. 5E, body weight loss in the DSS + miR-5106 group was significantly reduced compared to the DSS + miR-NC group starting from Day 5. The DAI of the DSS + miR-5106 group remained consistently lower than that of the DSS + miR-NC group from Day 4 (Fig. 5F). Additionally, colon lengths in the DSS + miR-5106 group were longer than those in the DSS + miR-NC group (Fig. 5G, H). The DSS + miR-5106 group also exhibited significantly lower macroscopic colon scores and less colonic architectural disruption compared to the DSS + miR-NC group (Fig. 5I, J). Consistently, histological scores were lower in miR-5106-treated colitis mice (Fig. 5K). Furthermore, goblet cell depletion induced by DSS was alleviated following Cc-ELNs treatment (Fig. 5L, M). Notably, the therapeutic efficacy of miR-5106 proved comparable to Cc-ELNs treatment (Fig. 5E-M). These findings suggest that Cc-ELNs protect against DSS-induced colitis by delivering high levels of miR-5106.

MiR-5106 delivery by Cc-ELNs inhibits neutrophil infiltration and NET formation in colitis mice

To determine whether miR-5106 plays a crucial role in Cc-ELNs-mediated inhibition of neutrophil infiltration and NET formation, we evaluated neutrophil levels in the intestinal mucosa and spleens of treated mice. MiR-5106 treatment resulted in a significant reduction in neutrophil infiltration (Fig. 6A). The percentage of neutrophils in the spleens of miR-5106-treated mice was significantly lower than in miR-NC-treated colitis mice (Fig. 6B, C). Moreover, miR-5106 treatment substantially reduced NET formation in the intestinal mucosa of colitis mice compared to miR-NC treatment (Fig. 6D). Further, neutrophils isolated from the BM and spleen of colitis mice after 24 h of in vitro culture exhibited significantly reduced NET formation with miR-5106 treatment (Fig. 6E-H). Neutrophils from miR-5106-treated mice formed fewer NETs when stimulated by PMA compared to those from miR-NC-treated colitis mice (Figure S7A-D). These results indicate that miR-5106 delivered by Cc-ELNs inhibits neutrophil infiltration and NET formation in colitis mice.

MiR-5106 inhibits NET formation by targeting Slc39a2 to restore intracellular zinc homeostasis

To elucidate the molecular mechanism by which miR-5106 inhibits NET formation, we identified direct target genes regulated by miR-5106. Using Miranda, we predicted potential miR-5106 targets, and among the top 10 (ranked by score), only Slc39a2 in the colon of colitis mice was significantly down-regulated after treatment with Cc-ELNs and miR-5106 (Fig. 7A, Figure S8). The miR-5106-binding site on the 3′-UTR of Slc39a2 is shown in Fig. 7B. To confirm that Slc39a2 is a direct target of

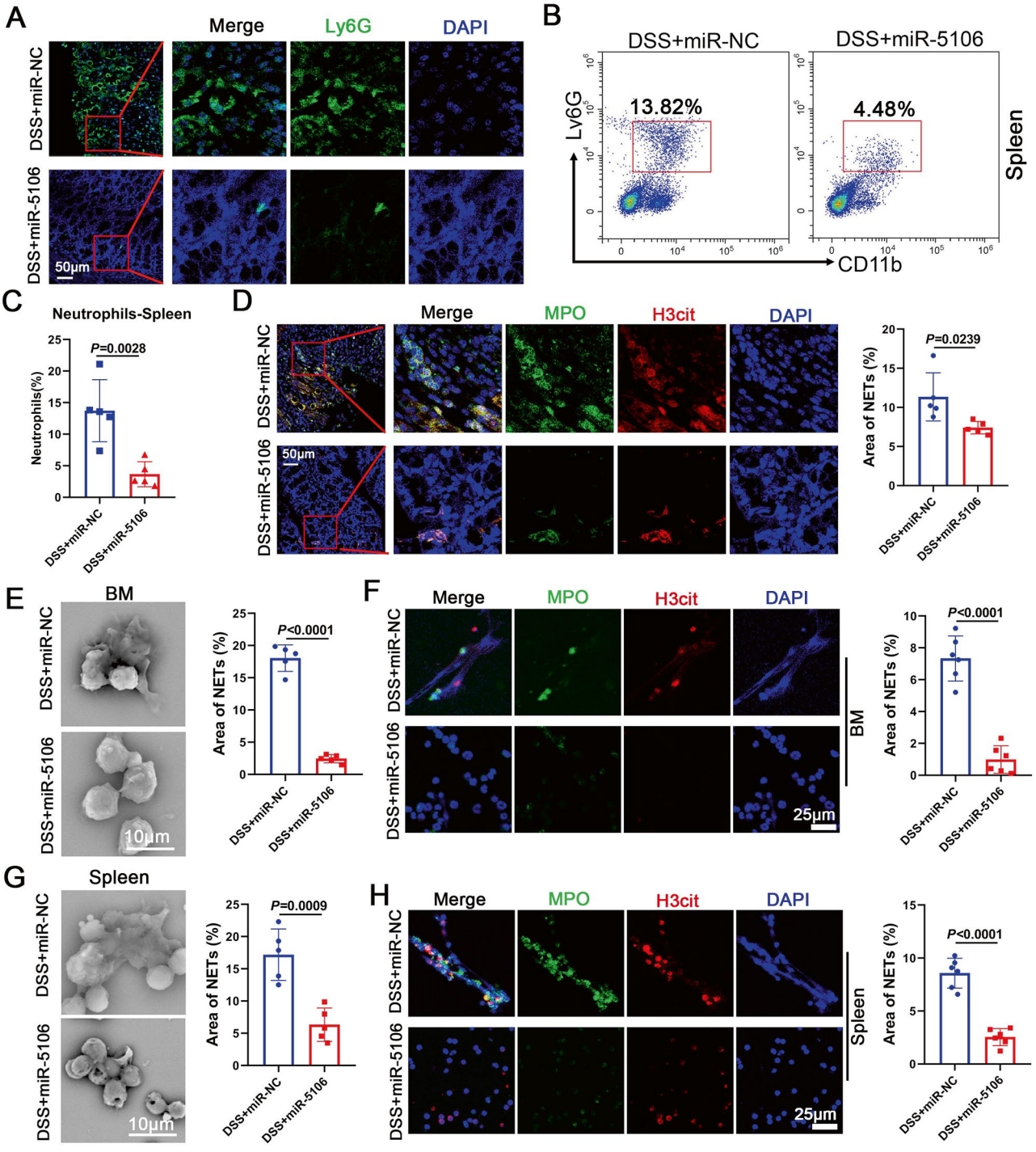

Fig. 6 MiR-5106 delivery by Cc-ELNs inhibits neutrophil infiltration and NET formation in colitis mice. (**A**) Immunofluorescence analysis was performed to assess neutrophil counts in colon tissues. (**B**, **C**) Percentage of neutrophils in the spleen was determined using flow cytometry (**B**), and the results of statistical analysis are shown (**C**). (**D**) Immunofluorescence was used to evaluate NET formation in the colon tissues of colitis mice. (**E**–**H**) Neutrophils isolated from the BM and spleen of mice were cultured in vitro for 24 h. SEM and immunofluorescence analyses were performed to assess NET formation. $n = 5–6$; Statistical significance was determined using unpaired two-sample *t*-test

miR-5106, we constructed a luciferase reporter plasmid containing the 3′-UTR of Slc39a2, along with a mutated version of the miR-5106 binding site. Dual-luciferase reporter assays demonstrated that miR-5106 significantly reduced luciferase activity in the wild-type Slc39a2 construct but had no effect on the mutated version (Fig. 7C).

Zinc transporters, encoded by the Slc300 and Slc39 gene families, are essential for maintaining intracellular

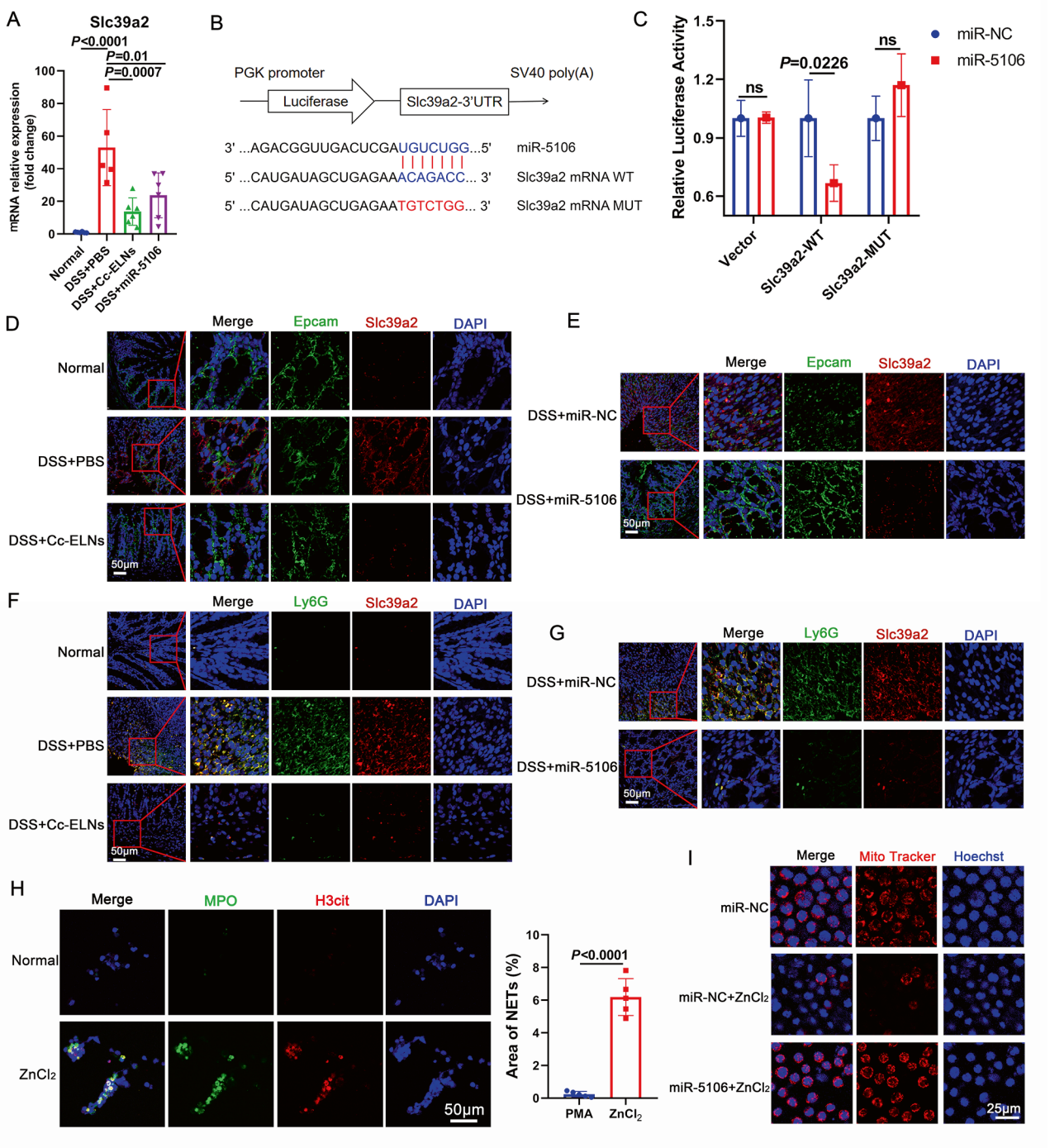

Fig. 7 miR-5106 inhibits NET formation by targeting Slc39a2 to restore intracellular zinc homeostasis. (**A**) Slc39a2 mRNA expression was analyzed using qRT-PCR. (**B**) Wild-type and mutated m-Slc39a2-3′-untranslated region (UTR) was cloned into pmirGLO, and the predicted binding site of miR-5106 in the 3′-UTR of the Slc39a2 gene. (**C**) HEK293T cells were transfected with the Slc39a2 UTR reporter plasmid along with miR-5106 mimic or miR-NC mimic. Dual-luciferase reporter assays were performed to measure the impact of miR-5106 on Slc39a2 expression. (**D**–**G**) Immunofluorescence analyses were performed to detect Slc39a2 expression in intestinal epithelium and neutrophils in the colon. (**H**) Neutrophils were treated with $ZnCl_2$, and NET formation was evaluated using immunofluorescence assay. (**I**) Neutrophils were treated with miR-NC, miR-NC + $ZnCl_2$, and miR-5106 + $ZnCl_2$, and the mitochondrial situation was evaluated using the Mito Tracker Red fluorescent probe. $n = 5–6$; Statistical significance was determined using one-way ANOVA followed by Tukey's multiple comparison test (**A**) and unpaired two-sample *t*-test (**C**, **H**)

zinc homeostasis [38–40]. While Slc300 transporters lower cytoplasmic zinc, Slc39 transporters increase intracellular zinc by facilitating its uptake [39]. Slc39a2, in particular, plays a key role in zinc transport [41]. We hypothesized that elevated Slc39a2 expression in colitis mice disrupts zinc homeostasis, contributing to NET formation, whereas Cc-ELNs can alleviate this condition by delivering miR-5106. To test this, we measured Slc39a2 expression levels in intestinal epithelium of mouse colon tissues. We found that Slc39a2 expression was significantly increased in intestinal epithelium of colitis mice, exacerbating epithelial damage, while treatment with Cc-ELNs and miR-5106 downregulated Slc39a2 expression and alleviated epithelial injury (Fig. 7D, E). Furthermore, we observed high Slc39a2 expression in neutrophils within colon tissues of colitis mice, and both Cc-ELNs and miR-5106 treatments markedly reduced neutrophil infiltration and Slc39a2 expression (Fig. 7F, G). To further validate this mechanism, neutrophils were treated with $ZnCl_2$ to elevate intracellular zinc levels and observed a significant increase in NET formation (Fig. 7H). Mitochondria, which play a pivotal role in NET formation by releasing reactive oxygen species (ROS) [42], were damaged by $ZnCl_2$-induced zinc overload. This resulted in reduced mitochondrial abundance and increased ROS production in neutrophils (Fig. 7I, Figure S9). However, treatment with miR-5106 mitigated mitochondrial damage (Fig. 7I). These findings suggest that elevated Slc39a2 expression in colitis mice promotes excessive zinc accumulation in neutrophils, leading to NET formation through mitochondrial destruction. By targeting Slc39a2, miR-5106 delivered by Cc-ELNs restores zinc homeostasis and inhibits NET formation.

In vivo safety of Cc-ELNs

To determine the systemic safety of Cc-ELNs administration, mice were intraperitoneally injected with Cc-ELNs for 7 consecutive days (Fig. 8A). Throughout the treatment period, all animals appeared healthy, with no significant differences in body weight observed (Fig. 8B). Organ indices showed no statistically significant differences between the Normal + PBS and Normal + Cc-ELNs groups (Fig. 8C). Compared to the Normal + PBS group, Cc-ELNs treatment did not alter liver function parameters [alanine aminotransferase (ALT), aspartate aminotransferase (AST), total protein (TP)] or renal function-related indices [creatinine (CREA), carbamide (UREA)] (Fig. 8D, E). To further investigate potential hepatorenal toxicity, mice were sacrificed after 7 days of intraperitoneal Cc-ELNs administration, and tissues were collected. H&E staining analysis revealed no damage to the liver, kidney, spleen, heart, lung, brain, or BM, and intestinal sections displayed no abnormalities (Fig. 8F, G). These results suggest that intraperitoneal injection of Cc-ELNs is safe.

Discussion

In this study, we demonstrated that Cc-ELNs alleviate DSS-induced colitis by reducing neutrophil recruitment and inhibiting NET formation. Our results show that NETs inhibit IEC and ISC proliferation while promoting IEC pyroptosis in colitis mice. However, Cc-ELNs counteract these effects by inhibiting NET formation. Mechanistically, Cc-ELNs deliver miR-5106, which targets and suppresses Slc39a2 expression, thereby restoring zinc homeostasis in neutrophils and reducing NET formation (Fig. 9).

Current treatments for IBD include glucocorticoids, antibiotics, and biologics (e.g., anti-TNFα, anti-IL-12/23). However, these therapies fail to cure IBD, requiring lifelong management to prevent or delay disease progression. Thus, there is an urgent need to search alternative therapeutic strategies. EVs exhibit advantages such as circulatory stability, high biocompatibility, low immunogenicity, and enrichment in bioactive components (e.g., lipids, proteins, and miRNAs). Recent studies highlight the potential of P-ELNs in treating colitis and other diseases. Negatively charged P-ELNs can penetrate the mucus layer to reach inflamed intestinal regions and serve as carriers for targeted delivery of chemical or nucleic acid drugs [43]. These unique properties make P-ELNs superior to traditional herbal medicine approaches. Therefore, we investigated the therapeutic effects of Cc-ELNs and their encapsulated miR-5106 in alleviating colitis, suggesting their potential for clinical application. In addition, we systematically evaluated the systemic safety profile of Cc-ELNs through toxicological assessments, and demonstrated excellent biocompatibility, which highlighted the promising therapeutic potential of Cc-ELN for the treatment of IBD.

BBR has previously demonstrated protective effects in colitis models. In this study, BBR was used as a positive control at an equivalent dose to Cc-ELNs. We found that the Cc-ELNs group exhibited a smaller trend of weight loss compared to the BBR group. Furthermore, the macroscopic colon scores in the DSS + Cc-ELNs group were lower than those in the DSS + BBR group. Collectively, based on indicators such as body weight loss, colon length, and macroscopic colon scores, the therapeutic effects of Cc-ELNs surpassed those of BBR. These findings suggest that BBR is not the primary component responsible for the therapeutic efficacy of Cc-ELNs, which instead function through other constituents.

Neutrophils, key mediators of innate immunity, are crucial for initiating acute inflammatory responses and serving as the first line of defense against pathogens [6]. Colitis pathogenesis is characterized by increased

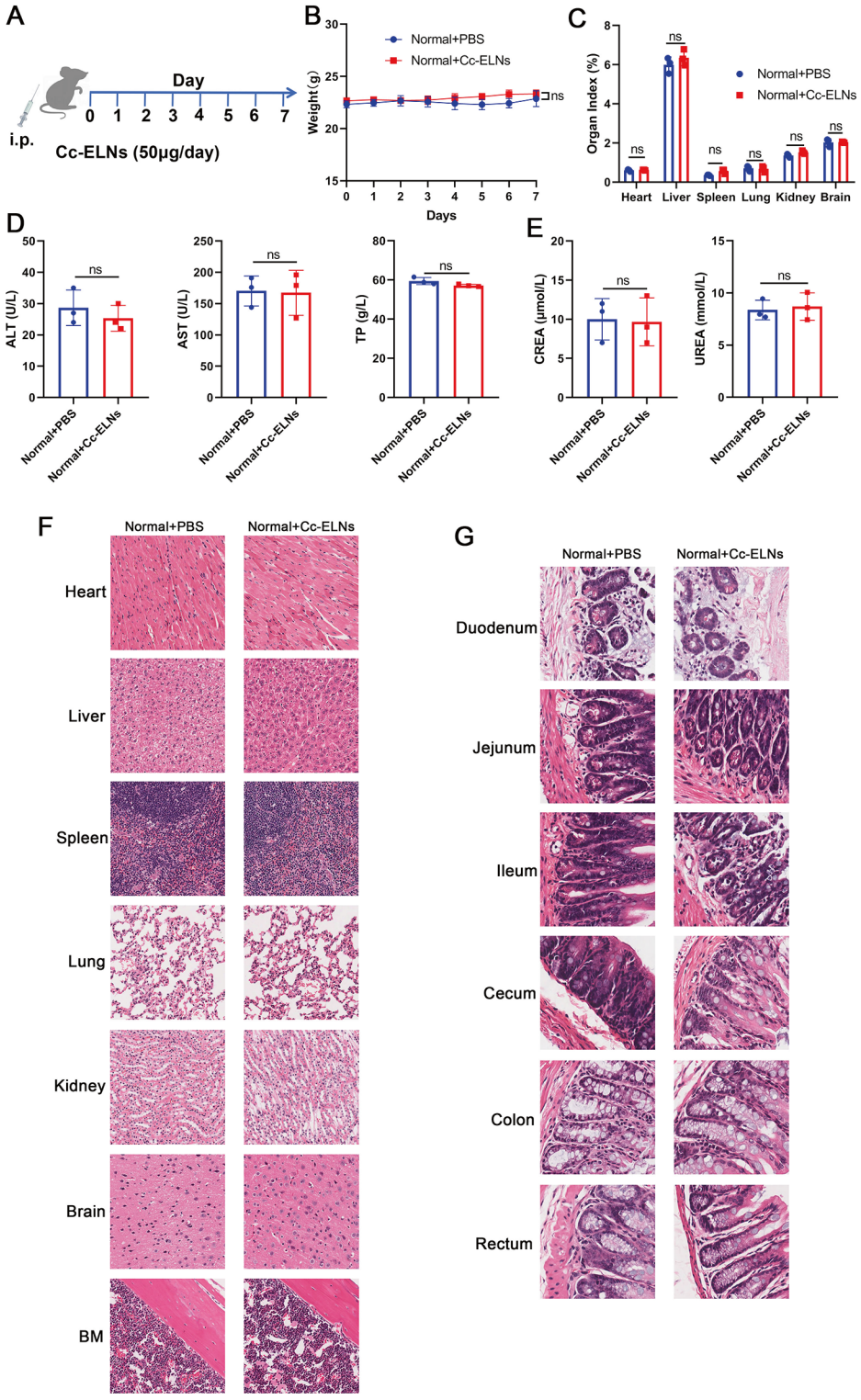

Fig. 8 Safety assays for Cc-ELNs. (**A**) Schematic of intraperitoneal Cc-ELNs administration. (**B**) Body weight variations in mice. (**C**) Organ indices (organ weight/body weight×100%). (**D**, **E**) Serological indices of liver (**D**) and kidney function (**E**). (**F**) Representative images of H&E-stained heart, liver, spleen, lung, kidney, brain, and BM sections. (**G**) H&E staining of intestinal segments (duodenum, jejunum, ileum, cecum, colon, and rectum). $n = 3$; Statistical significance was determined using an unpaired two-sample *t*-test

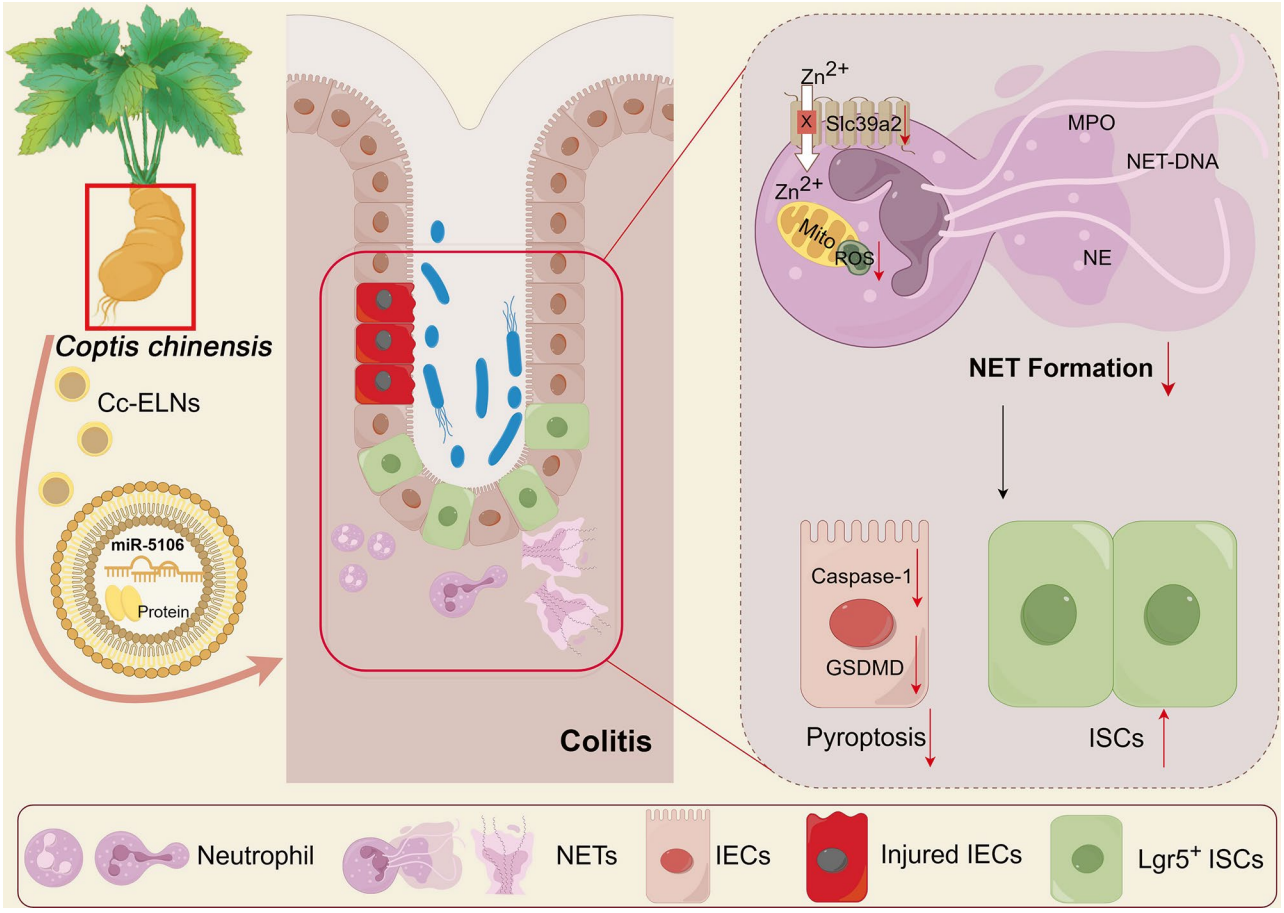

Fig. 9 Schematic diagram of the experimental study. Cc-ELNs effectively alleviated colitis by reducing neutrophil recruitment and inhibiting NET formation. Cc-ELNs inhibited pyroptosis in IECs and promoted the proliferation of IECs and ISCs by reducing NETs. Mechanistically, miR-5106 delivery by Cc-ELNs inhibited NET formation by targeting Slc39a2 to restore intracellular zinc homeostasis

cytokine production and the local accumulation of immune cells, particularly neutrophils, which contribute to tissue damage, crypt destruction, and the formation of crypt abscesses [44]. We found that Cc-ELNs were distributed in intestinal tissues. Cc-ELNs were found throughout the jejunum, ileum, cecum, and colon. The selective accumulation of Cc-ELNs in inflamed colonic regions may be attributed to multiple mechanisms. First, the enhanced permeability and retention (EPR) effect. In IBD, the disrupted vascular endothelium and increased interstitial fluid pressure may allow nanoparticles to extravasate and accumulate in diseased areas. Second, Cc-ELNs may harbor surface ligands derived from *Coptis chinensis* that actively bind to receptors overexpressed in inflamed intestines. However, further studies are needed to identify specific ligands and their targets. Additionally, literature suggests that negatively charged plant-derived exosomes can penetrate the mucus layer via electrostatic interactions to reach inflamed intestinal regions [43]. Finally, interactions with immune cells could further enhance targeting. We observed that Cc-ELNs were internalized by neutrophils.

Our study found that Cc-ELNs reduced neutrophil recruitment from the bone marrow to peripheral organs, including the colon, spleen, and Peyer's patches, in mice with colitis. Neutrophils employ various mechanisms to neutralize pathogens, including phagocytosis, antimicrobial secretion, and NET formation. While NETs are effective in trapping and killing bacteria due to their high concentration of histones and granule-derived enzymes, they are also implicated in pathological sterile inflammation, such as in cancer and autoimmune diseases [45]. Their therapeutic potential is being actively explored. NET formation is elevated in DSS-induced colitis and contributes to thrombus formation via NET-dependent pathways [9]. Inhibition of NET formation in colitis mice significantly alleviates disease progression [46, 47]. Our findings suggest that Cc-ELNs effectively alleviate colitis by not only reducing neutrophil recruitment but also suppressing NET formation.

Currently, no cure exists for IBD, and current treatments focus primarily on symptom management and long-term remission [48]. A critical physiological process in the recovery from colitis and maintenance of intestinal homeostasis is the resolution of inflammation, where IECs play a pivotal role through their interaction with the mucosal immune system and local microenvironment [49]. Despite the lack of treatments specifically aimed at enhancing intestinal barrier function, the intestinal epithelium remains a promising therapeutic target for IBD [50]. Our findings show that NETs inhibit IEC proliferation, whereas Cc-ELNs, by inhibiting NET formation, promote IEC proliferation. Gasdermins (GSDMs), particularly GSDMD, are key mediators of pyroptosis, and GSDMD's pore-forming ability, triggered by cleavage and oligomerization, has significantly advanced our understanding of programmed cell death [51]. In our study, NETs upregulated GSDMs in IECs, but Cc-ELNs markedly downregulated their expression by inhibiting NET formation. These results suggest that Cc-ELNs foster IEC proliferation and inhibit pyroptosis by blocking NET formation. To maintain tissue homeostasis, the intestinal epithelium undergoes continuous regeneration through the rapid proliferation and differentiation of ISCs into specific IEC subtypes [52]. We observed a notable reduction in ISC numbers in colitis mice, likely due to mucosal destruction; however, ISC populations were restored following NET inhibition via DNase I or Cc-ELNs, highlighting the potential of Cc-ELNs to promote intestinal regeneration. We found that miR-5106 is highly expressed in Cc-ELNs, and its administration significantly alleviates colitis in mice, suggesting that miR-5106 is a key component of Cc-ELNs' therapeutic effect in enteritis.

The intestine is a major site for zinc absorption and excretion, and maintaining zinc homeostasis is crucial for the integrity of the intestinal mucosal barrier [53]. Both zinc deficiency and excess are associated with various intestinal diseases, including IBD and colorectal cancer [53]. Zinc deficiency disrupts cellular function, while excess zinc can be toxic. High dietary zinc exacerbates *Clostridium difficile* infection by enhancing bacterial toxicity and altering host immune responses [54]. In our study, we observed that the zinc transporter Slc39a2, which facilitates intracellular zinc uptake, is significantly upregulated in the colons of colitis mice. miR-5106, delivered by Cc-ELNs, directly targets and inhibits Slc39a2 expression. Moreover, we found that excess zinc induces NET formation. NET formation is triggered by innate immune receptors and downstream intracellular mediators, including ROS, generated by NADPH oxidase or mitochondria. Ribonucleoprotein immune complexes, inducers of NETosis, require ROS for maximal NET stimulation [42]. These ROS activate myeloperoxidase (MPO), neutrophil elastase (NE), and protein arginine deiminase type 4 (PAD4), which promote chromatin decondensation [8]. The activation of ROS-PAD4 pathway promotes uncontrolled NET formation [55]. Mitochondrial damage leads to ROS release, further driving NET formation. Our results demonstrate that ZnCl2 induces mitochondrial damage in neutrophils, reducing mitochondrial abundance, whereas miR-5106 mitigates these effects by downregulating Slc39a2. These findings suggest that miR-5106 regulates intracellular zinc homeostasis by targeting Slc39a2, thereby suppressing NET formation. However, further studies are required to fully elucidate the underlying molecular mechanisms.

Conclusions

In summary, our study identifies Cc-ELNs and their high miR-5106 content as potent modulators of neutrophil function, significantly reducing neutrophil recruitment and NET formation, thereby alleviating colitis. By targeting zinc homeostasis in neutrophils through Slc39a2, miR-5106 plays a pivotal role in regulating inflammation and promoting intestinal epithelial recovery. These findings highlight the therapeutic potential of P-ELN miRNAs in the treatment of IBD.

Materials and methods

Isolation and characterization of Cc-ELNs

Cc-ELNs were isolated from *Coptis chinensis* juice using a multi-step differential centrifugation protocol. Fresh *Coptis chinensis* was homogenized to obtain juice, which was subjected to sequential centrifugation at 1,000 *g* (10 min), 3,000 *g* (20 min), and 10,000 *g* (30 min) to remove large fibers. The resulting supernatant was filtered through a 0.22-μm membrane and ultracentrifuged at 120,000 *g* for 60 min (Optima L-100xp, Beckman Coulter, USA). The pellet was resuspended in PBS, and Cc-ELNs were quantified by protein content using a bicinchoninic acid protein assay kit (Beyotime, China). Samples were stored at – 80 °C until further analysis.

The morphology of Cc-ELNs was examined using transmission electron microscopy (TEM). Briefly, Cc-ELNs were deposited onto a copper grid, stained with 3% (w/v) aqueous phosphotungstic acid for 1 min, and examined using a JEM-1400PLUS (Jeol, Japan). Cc-ELNs were also characterized using high-sensitivity flow cytometry for nanoparticle analysis (N30, NanoFCM, China).

Animals and ethics

Six-week-old male C57BL/6J mice were purchased from the Guangdong Medical Laboratory Animal Center, China. All animal procedures followed the guidelines set by the Animal Care and Use Committee of Guangzhou Medical University (approval number: G2023-726) and complied with the National Institutes of Health

Guidelines for the Care and Use of Laboratory Animals in China.

In vivo biodistribution of Cc-ELNs

To assess the in vivo biodistribution of Cc-ELNs, the particles were labeled with DiR fluorescent dye (UElandy, China) by incubating at 37 °C for 30 min, following the manufacturer's instructions. The solution was ultracentrifuged at 120,000 *g* for 90 min at 4 °C, and the pellet was resuspended in 200 μL of PBS to obtain DiR-Cc-ELNs. Mice were intraperitoneally injected with 150 μg of DiR-Cc-ELNs per mouse and euthanized 24 h later. Tissues from the intestine, femur, heart, liver, spleen, lungs, kidneys, and brain were collected for ex vivo imaging analysis to monitor Cc-ELN biodistribution. DiR fluorescent signals were detected using the Odyssey CLx (LI-COR Biosciences, USA).

Induction of DSS colitis and treatment

Acute colitis was induced by administering 2.5% (wt/vol) dextran sulfate sodium (DSS, 36–50 kDa, MP Biomedicals) in drinking water for 8 days consecutively (days 0–7). Mice were randomly assigned to the following groups: Normal, DSS, DSS + Cc-ELNs, DSS + BBR, DSS + DNase I, DSS + miR-NC (RIBOBIO, China), and DSS + miR-5106 (RIBOBIO, China). The intervention groups received intraperitoneal injections of Cc-ELNs (50 μg per mouse), BBR (50 μg per mouse), DNase I (20 mg/kg), miR-NC (5 nmol per mouse), or miR-5106 (5 nmol per mouse), respectively. Control groups (normal and DSS) received equivalent volumes of PBS through intraperitoneal injection.

Clinical and histological evaluation of colitis

Disease progression was monitored daily by evaluating body weight changes, stool consistency, and the presence of fecal blood using a hemoccult assay kit (Nanjing Jiancheng Bio-engineering Institute, China). DAI was calculated based on these parameters, following established protocols [56].

On day 7, mice were euthanized, and colon lengths were measured. A blinded observer performed macroscopic evaluation of the colons, considering factors such as hyperemia, wall thickening, ulceration, extent of inflammation, and overall damage (Table 1) [56]. Colonic tissues were fixed in 4% paraformaldehyde, processed, and embedded in paraffin. Sections were stained with hematoxylin and eosin (H&E) for histopathological analysis, including the assessment of inflammation severity, immune cell infiltration, crypt damage, submucosal edema, goblet cell loss, and epithelial hyperplasia [56].

Table 1 Assessment of macroscopic scores

Score	The damage of colon
0	No damage
1	Hyperemia without ulcers
2	Hyperemia and wall thickening without ulcers
3	One ulceration site without wall thickening
4	Two or more ulceration sites
5	0.5 cm extent of inflammation or major damage
6–10	1 cm extent of inflammation or severe damage

Goblet cell quantification

Alcian blue-periodic acid Schiff (AB-PAS) staining was used to visualize and quantify goblet cells in colon sections. The number of goblet cells per crypt was quantified.

Flow cytometric analysis of neutrophil subsets

Neutrophil subsets were analyzed in cells isolated from Peyer's patches, spleens, and femoral BM. Single-cell suspensions were stained with fluorochrome-conjugated monoclonal antibodies targeting CD11b and Ly6G (BioLegend, USA), following the manufacturer's instructions. Data acquisition was performed using a CytoFLEX S flow cytometer (Beckman Coulter, USA), and neutrophil populations were quantified using CytExpert software (Beckman Coulter, USA).

Neutrophil isolation and in vitro treatments

Neutrophils were isolated from the femur, tibia, and spleens of mice using Percoll density gradient centrifugation. Isolated neutrophils were cultured at 37 °C in a 5% CO_2 humidified atmosphere. For in vitro experiments, neutrophils were seeded on coverslips and treated for 24 h with Cc-ELNs (20 μg/mL), BBR (20 μg/mL), miR-NC (20 μM), miR-5106 (20 μM), or $ZnCl_2$ (200 μM). PMA (150 nM) was added 4 h before cell collection to stimulate NET formation.

Immunofluorescence analysis

For immunofluorescence analysis of colon tissue sections, specimens were fixed, embedded in paraffin, and sectioned. Sections were deparaffinized, rehydrated, and blocked with 1% bovine serum albumin. The samples were incubated overnight at 4 °C with the following primary antibodies: anti-MPO (1:100; Abcam, UK), anti-H3cit (1:200; CST, USA), anti-Ki67 (1:500; Abcam, UK), anti-GSDMD (1:100; Proteintech, China), and anti-Lgr5 (1:200; Abcam, UK). For cultured cell analysis, cells were fixed with 4% paraformaldehyde for 25 min at room temperature, permeabilized with 0.1% Triton X-100 in PBS for 4 min, and blocked with PBS containing 2% BSA for 30 min. The cells were incubated overnight at 4 °C with anti-MPO (1:100; Abcam, UK), anti-H3Cit (1:200; CST, USA), anti-Ki67 (1:500; Abcam, UK), anti-GSDMD (1:100; Proteintech, China), Mito-Tracker Red CMXRos (50 nM; Beyotime, China), 2′,7′-dichlorofluorescein

diacetate (DCFH-DA) probes (1 μM; Solarbio, China), and Hoechst (1:2000; Beyotime, China). Both tissue sections and cells were incubated with appropriate Alexa Fluor-conjugated secondary antibodies. Nuclear staining was achieved with DAPI. Samples were washed three times with PBS, each wash lasting 1 min, and visualized using a TCS SP8 DLS laser scanning confocal microscope (Leica, Germany).

Scanning electron microscopy

Neutrophils cultured on coverslips were fixed with 2.5% glutaraldehyde overnight. After fixation, samples were washed with PBS and dehydrated using an ethanol gradient, followed by exchange with acetone and isoamyl acetate. Specimens were subjected to critical point drying and gold coating using an ion coater. Imaging was performed using a TM4000Plus II scanning electron microscope (HITACHI, Japan).

Analysis of Cc-ELNs uptake

Cc-ELNs were labeled with PKH26 fluorescent dye (MCE, China) for 5 min, after which an equal volume of 1% BSA was added to terminate the staining. The labeled Cc-ELNs were transferred to a Quick-Seal centrifuge tube (Beckman Coulter, USA) and ultracentrifuged at 120,000 g for 90 min at 4 °C using an Optima L-100xp ultracentrifuge with a swinging-bucket rotor (SW60 Ti, Beckman Coulter). The resulting pellet containing PKH26-labeled Cc-ELNs was resuspended in PBS and underwent a second round of ultracentrifugation under identical conditions to ensure purity.

To assess internalization, neutrophils were incubated with the purified PKH26-labeled Cc-ELNs for 1 h, and prepared for confocal microscopy analysis. Alexa Fluor phalloidin-FITC (CST, USA) was used to label actin, and DAPI was used to detect nuclei.

Purification of NETs and NETs-DNA and mouse IECs treatment

NETs were collected from freshly isolated mouse neutrophils as described previously with minor modifications [35]. Neutrophils were stimulated with 500 nM PMA for 4 h, after which the supernatant was discarded. NETs adhering to the container bottom were resuspended by gently pipetting 2 mL of chilled PBS. NETs were centrifuged at 1,000 *g* for 10 min at 4 °C. The cell-free supernatant containing the NETs (a DNA-protein complex) was carefully collected. NET-DNA was purified using a MicroElute DNA Clean Up Kit (OMEGA, China), and its concentration was determined by spectrophotometry. Mouse IECs were stimulated with 2.5 μg/mL of NETs or NET-DNA, and the expression of Ki67 and GSDMD was assessed by immunofluorescence.

Small RNA sequencing and analysis

Small RNA sequencing was conducted as previously described [57]. Total RNA was extracted from Cc-ELNs and used for small RNA library preparation. Following cluster generation, libraries were sequenced on an Illumina NovaSeq 6000 platform (Illumina, USA). Data analysis included quality control, comparative analysis, target gene functional annotation, and quantification of miRNA expression levels.

Prediction of potential miR-5106 target genes and dual-luciferase reporter assay

The miRanda algorithm was used to predict potential targets of miR-5106. Target genes were selected based on scores and conserved binding sites identified by miRanda. HEK293T cells were transfected with reporter plasmids encoding either the un-mutated or mutated 3′-UTR of Slc39a2, along with miR-5106 mimic or control mimic, for 48 h using RNAiMAX (Invitrogen). Luciferase activity was measured with a luciferase assay reagent (Beyotime, China) using an Infinite Synergy H1 plate reader (Agilent, USA), and normalized to Renilla luciferase activity.

RNA extraction and qRT-PCR

mRNA expression was quantified using qRT-PCR. Briefly, RNA was extracted from cells by homogenizing 100 mg of colon tissues in TRIzol reagent (Invitrogen, USA) following the manufacturer's guidelines. The extracted RNA was quantified using a NanoDrop ND-2000 spectrophotometer (Thermo Scientific, USA). Complementary DNA (cDNA) was synthesized from 1.0 mg of total RNA using oligo (dT) primers and a Thermo Scientific RevertAid First Strand cDNA synthesis kit (Thermo Scientific), adhering to the manufacturer's protocol. Expression of GSDMD, Caspase-1, Usp49, Trim66, Slc39a2, Krt84, Epb42, and Col28a1, Ccdc130, P2rx2, Ksr2, Zbtb34 and Selp was analysed using a SYBR Green Master Mix kit (Takara, Japan) with the primers listed in Table 2. GAPDH served as the internal control, and the fold-change in expression was calculated using the $2^{-\Delta\Delta CT}$ method.

Serum analysis

Blood samples from mice were allowed to clot at room temperature for 1 h and then centrifuged at 3000 rpm for 15 min to obtain serum. Liver function parameters (ALT, AST, and TP) as well as renal function-related indices (CREA and UREA) were measured using commercial assay kits (Kehua Bio-engineering, Shanghai, China) according to the manufacturer's protocols.

Statistical analysis

Results are presented as mean ± SD. Comparisons between two groups were performed using unpaired

Table 2 Primers used for qRT-PCR

Gene	Forward (5′-3′)	Reverse (5′-3′)
GSDMD	TACTGCCTTCTGAACAGGAA	GTCACCACAAACAGGTCATC
Caspase-1	ACACGTCTTGCCCTCATTATCT	ATAACCTTGGGCTTGTCTTTCA
Usp49	AGTTCCGGGAATGTTTCCTGA	CTCCTTACTGACAACTCTGCG
Trim66	GCAAGCCAACGGGCTCATA	GGAAAGGGACGCTGCTTTTG
Slc39a2	TACGTGGAGTATCCCTATGGAGA	GAGTCCCTCCCCATTCCTCT
Krt84	TCTTGCCGCTCCTACAGAGT	GACGCTCCGACTACCAAAACC
Epb42	CCACGCAGCAGAAAACAACG	GAGCACGGAAGTTCAGGGT
Col28a1	AGCAGCGGGTCAAGTCTCT	ACGCCATCTTTACGCCCTTC
P2rx2	GCGTTCTGGGACTACGAGAC	CGTACCACACGAAGTAAAGCA
Ccdc130	CATGGCTCTCTCAACCGATAC	CATGCCGATGTGGTTCTTACA
Ksr2	GAGGAAAACATGACGAAAAGCG	TGAGGTCGTTGGAAGCTGC
Selp	CCGGAGTGTGATCCTGGGA	TGTGCTGTAGTTATAGGTCCACG
Zbtb34	TCAAGATTACGTTTCGTGTCGG	TGAATGGTCCCGGAAATACGG
GAPDH	ACTCCACTCACGGCAAATTC	TCTCCATGGTGGTGAAGACA

two-sample *t*-tests. For multiple comparisons involving more than two groups, one-way ANOVA followed by Tukey's multiple comparison tests was employed. *P* values < 0.05 were deemed statistically significant. Quantification of immunofluorescence and scanning electron microscopy data was carried out using ImageJ software. All statistical analyses were conducted using GraphPad Prism 8.0.

Abbreviations

IBD	Inflammatory bowel disease
ELNs	Extracellular vesicle-like nanoparticles
Cc-ELNs	Coptis chinensis-derived ELNs
DSS	Dextran sulfate sodium
NETs	Neutrophil extracellular traps
IECs	Intestinal epithelial cells
ISCs	Intestinal stem cells
EVs	Extracellular vesicles
P-ELNs	ELNs from plants
BBR	Berberine
TEM	Transmission electron microscopy
DAI	Disease Activity Index
H&E	Hematoxylin and eosin
AB-PAS	Alcian blue-periodic acid Schiff
PMA	Phorbol 12-myristate 13-acetate
GSDMD	Gasdermin D
BM	Bone marrow
SEM	Scanning electron microscopy
NETs-DNA	NETs consist of chromatin DNA filaments
miRNAs	MicroRNAs
ROS	Reactive oxygen species
UTR	Untranslated region
GSDMs	Gasdermins
BMSCs	Bone mesenchymal stem cells
MPO	Myeloperoxidase
NE	Neutrophil elastic enzyme
PAD4	Protein arginine deiminase type 4

Supplementary Information

The online version contains supplementary material available at https://doi.org/10.1186/s12951-025-03466-z.

Supplementary Material 1

Author contributions

Y. Y. (Yi Yang)and L. Y. were responsible for the experimental design, data collection, and initial analysis of the results. H. D., Y. L. and J. W. conducted the experiments and managing the laboratory resources. Y. Y. (Yilin Yang), J. S. and S. S. were in charge of the data interpretation and statistical analysis. J. X., J. W., X. D., and Y. W. assisted with the preparation of figures and tables for the manuscript. Y. L. and L. W. provided overall guidance, conceptual advice, and wrote the manuscript. All authors read and approved the final manuscript.

Funding

This work was supported by the Science and Technology Plan Project of Guangzhou (No. 2023A04J0559), the Guangzhou Basic and Applied Basic Research Foundation (No. SL2023A04J02525), the Postdoctoral Fellowship Program of China Postdoctoral Science Foundation (No. GZC20230601), the Department of Education of GuangDong Province (No. 2023ZDZX2048), the National Natural Science Foundation of China (No. 81902081), the Natural Science Foundation of Guangdong Province (Nos. 2020A1515011573, 2023A1515220167), Open Project of Guangzhou Medical University, Guangzhou Science and Technology Fund (No. 2024A03J0791), and the Youth Innovation Talent Project of Ordinary university in Guangdong Province (No. 2022KQNCX061).

Data availability

No datasets were generated or analysed during the current study.

Declarations

Ethics approval and consent to participate

Ethics approval Animal protocols were approved by the Animal Care and Use Committee of Guangzhou Medical University (approval number: G2023-726) and complied with the National Institutes of Health Guidelines for the Care and Use of Laboratory Animals in China.

Consent for publication

All authors of this study agreed to publish.

Competing interests

The authors declare no competing interests.

Author details

[1]KingMed School of Laboratory Medicine, The Affiliated Traditional Chinese Medicine Hospital, Guangzhou Medical University, Guangzhou 511436, China
[2]Engineering Technology Research Center of Intelligent Diagnosis for Infectious Diseases in Guangdong Province, Guangzhou 511436, China
[3]Guangzhou Key Laboratory for Clinical Rapid Diagnosis and Early Warning of Infectious Diseases, Guangzhou 511436, China
[4]The Department of Clinical Laboratory, The Second Affiliated Hospital of Guangzhou Medical University, Guangzhou, China

Received: 24 December 2024 / Accepted: 14 May 2025
Published online: 14 June 2025

References

1. Massironi S, Viganò C, Palermo A, et al. Inflammation and malnutrition in inflammatory bowel disease. Lancet Gastroenterol Hepatol. 2023;8:579–90.
2. Rubin DT, Ananthakrishnan AN, Siegel CA, et al. ACG clinical guideline: ulcerative colitis in adults. Am J Gastroenterol. 2019;114:384–413.
3. Maloy KJ, Powrie F. Intestinal homeostasis and its breakdown in inflammatory bowel disease. Nature. 2011;474:298–306.

4. Zhou G, Yu L, Fang L, et al. CD177 + neutrophils as functionally activated neutrophils negatively regulate IBD. Gut. 2018;67:1052–63.
5. Mantovani A, Cassatella MA, Costantini C, Jaillon S. Neutrophils in the activation and regulation of innate and adaptive immunity. Nat Rev Immunol. 2011;11:519–31.
6. Kolaczkowska E, Kubes P. Neutrophil recruitment and function in health and inflammation. Nat Rev Immunol. 2013;13:159–75.
7. Wigerblad G, Kaplan MJ. Neutrophil extracellular traps in systemic autoimmune and autoinflammatory diseases. Nat Rev Immunol. 2023;23:274–88.
8. Papayannopoulos V. Neutrophil extracellular traps in immunity and disease. Nat Rev Immunol. 2017;18:134–47.
9. Zhang L, Zheng B, Bai Y, et al. Exosomes-transferred LINC00668 contributes to thrombosis by promoting NETs formation in inflammatory bowel disease. Adv Sci. 2023;10(28):e2300560.
10. Iannotta D, Amruta A, Kijas AW, et al. Entry and exit of extracellular vesicles to and from the blood circulation. Nat Nanotechnol. 2024;19:13–20.
11. Xia Y, Zhang J, Liu G, Wolfram J. Immunogenicity of extracellular vesicles. Adv Mater. 2024;36(33):e2403199.
12. Li N, Zhao L, Geng XY, et al. Stimulation by exosomes from hypoxia-preconditioned hair follicle mesenchymal stem cell s facilitates mitophagy by inhibiting the PI3K/AKT/mTOR signaling pathway to alleviate ulcerative colitis. Theranostics. 2024;14:4278–96.
13. Cong M, Tan S, Li S, et al. Technology insight: Plant-derived vesicles—How Far from the clinical biotherapeutics and therapeutic drug carriers? Adv Drug Deliv Rev. 2022;182:114108.
14. Rome S. Biological properties of plant-derived extracellular vesicles. Food Funct. 2019;10:529–38.
15. Zhang L, Li SM, Cong MH, et al. Lemon-Derived extracellular Vesicle-like nanoparticles block the progression of kidney stones by antagonizing Endoplasmic reticulum stress in renal tubular cells. Nano Lett. 2023;23:1555–63.
16. Yan G, Xiao QY, Zhao JY, et al. *Brucea javanica* derived exosome-like nanovesicles deliver MiRNAs for cancer therapy. J Controlled Release. 2024;367:425–40.
17. Kang SJ, Lee JH, Rhee WJ. Engineered plant-derived extracellular vesicles for targeted regulation and treatment of colitis-associated inflammation. Theranostics. 2024;14:5643–61.
18. Yan L, Cao YQ, Hou LH, et al. Ginger exosome-like nanoparticle-derived MiRNA therapeutics: A strategic inhibitor of intestinal inflammation. J Adv Res. 2025;69:1–15.
19. Lei C, Mu J, Teng Y, et al. Lemon Exosome-like Nanoparticles-Manipulated probiotics protect mice from *C. diff* infection. iScience. 2020;23(10):101571.
20. Ju SW, Mu JY, Dokland T, et al. Grape Exosome-like nanoparticles induce intestinal stem cells and protect mice from DSS-Induced colitis. Mol Ther. 2013;21:1345–57.
21. Zhu MZ, Xu HM, Liang YJ, et al. Edible exosome-like nanoparticles from *portulaca oleracea L* mitigate DSS-induced colitis facilitating double-positive CD4 CD8 T cells expansion. J Nanobiotechnol. 2023;21(1):309.
22. Kim J, Zhu Y, Chen SH, et al. Anti-glioma effect of ginseng-derived exosomes-like nanoparticles by active blood-brain-barrier penetration and tumor microenvironment modulation. J Nanobiotechnol. 2023;21(1):253.
23. Zhang L, He FJ, Gao LN, et al. Engineering Exosome-Like nanovesicles derived from can inhibit the proliferation of hepatocellular carcinoma cells with better safety profile. Int J Nanomed. 2021;16:1575–86.
24. Xie Q, Li H, Ma R, et al. Effect of *Coptis chinensis* Franch and Magnolia officinalis on intestinal flora and intestinal barrier in a TNBS-induced ulcerative colitis rats model. Phytomedicine. 2022;97:153927.
25. Lim S-M, Choi H-S, Kim D-H. The mixture of *Anemarrhena asphodeloides* and *Coptis chinensis* attenuates High-Fat Diet-Induced colitis in mice. Am J Chin Med. 2017;45:1033–46.
26. Zhou R, Huang Y, Tian C, et al. *Coptis chinensis* and Berberine ameliorate chronic ulcerative colitis: an integrated Microbiome-Metabolomics study. Am J Chin Med. 2023;51:2195–220.
27. Li H, Fan C, Lu HM, et al. Protective role of Berberine on ulcerative colitis through modulating enteric glial cells-intestinal epithelial cells-immune cells interactions. Acta Pharm Sinica B. 2020;10:447–61.
28. Jing WH, Dong SJ, Luo XL, et al. Berberine improves colitis by triggering AhR activation by microbial Tryptophan catabolites. Pharmacol Res. 2021;164:105358.
29. Yan SH, Chang JY, Hao XH, et al. Berberine regulates short-chain fatty acid metabolism and alleviates the colitis-associated colorectal tumorigenesis through remodeling intestinal flora. Phytomedicine. 2022;102:154217.
30. Kambe T, Tsuji T, Hashimoto A, Itsumura N. The physiological, biochemical, and molecular roles of zinc transporters in zinc homeostasis and metabolism. Physiol Rev. 2015;95:749–84.
31. Yin SH, Duan MP, Fang B, et al. Zinc homeostasis and regulation: zinc transmembrane transport through transporters. Crit Rev Food Sci Nutr. 2023;63:7627–37.
32. Danne C, Skerniskyte J, Marteyn B, Sokol H. Neutrophils: from IBD to the gut microbiota. Nat Reviews Gastroenterol Hepatol. 2024;21:184–97.
33. Broz P, Pelegrín P, Shao F. The gasdermins, a protein family executing cell death and inflammation. Nat Rev Immunol. 2020;20:143–57.
34. Miao R, Jiang C, Chang WY, et al. Gasdermin D permeabilization of mitochondrial inner and outer membranes accelerates and enhances pyroptosis. Immunity. 2023;56(11):2523–e25418.
35. Yang LB, Liu Q, Zhang XQ, et al. DNA of neutrophil extracellular traps promotes cancer metastasis via CCDC25. Nature. 2020;583:133–8.
36. Sorrentino G, Perino A, Yildiz E, et al. Bile acids signal via TGR5 to activate intestinal stem cells and epithelial regeneration. Gastroenterology. 2020;159:956–68.
37. Mori MA, Ludwig RG, Garcia-Martin R, et al. Extracellular MiRNAs: from biomarkers to mediators of physiology and disease. Cell Metabol. 2019;30:656–73.
38. Du L, Zhang H, Zhao H, et al. The critical role of the zinc transporter Zip2 (SLC39A2) in ischemia/reperfusion injury in mouse hearts. J Mol Cell Cardiol. 2019;132:136–45.
39. Liuzzi JP, Cousins RJ. Mammalian zinc transporters. Annu Rev Nutr. 2004;24:151–72.
40. Lichten LA, Cousins RJ. Mammalian zinc transporters: nutritional and physiologic regulation. Annu Rev Nutr. 2009;29:153–76.
41. Cousins RJ, Blanchard RK, Popp MP, et al. A global view of the selectivity of zinc deprivation and excess on genes expressed in human THP-1 mononuclear cells. Proc Natl Acad Sci. 2003;100:6952–7.
42. Lood C, Blanco LP, Purmalek MM, et al. Neutrophil extracellular traps enriched in oxidized mitochondrial DNA are interferogenic and contribute to lupus-like disease. Nat Med. 2016;22:146–53.
43. Yang S, Li W, Bai X, et al. Ginseng-derived nanoparticles alleviate inflammatory bowel disease via the TLR4/MAPK and p62/Nrf2/Keap1 pathways. J Nanobiotechnol. 2024;22(1):48.
44. Friedrich M, Pohin M, Powrie F. Cytokine networks in the pathophysiology of inflammatory bowel disease. Immunity. 2019;50:992–1006.
45. Herre M, Cedervall J, Mackman N, Olsson AK. Neutrophil extracellular traps in the pathology of Cancer and other inflammatory diseases. Physiol Rev. 2023;103:277–312.
46. Wang CPJ, Ko GR, Lee YY, et al. Polymeric DNase-I nanozymes targeting neutrophil extracellular traps for the treatment of bowel inflammation. Nano Convergence. 2024;11(1):6.
47. Qin D, Liu JX, Guo WW, et al. Arbutin alleviates intestinal colitis by regulating neutrophil extracellular traps formation and microbiota composition. Phytomedicine. 2024;130:155741.
48. Pouillon L, Travis S, Bossuyt P, et al. Head-to-head trials in inflammatory bowel disease: past, present and future. Nat Reviews Gastroenterol Hepatol. 2020;17:365–76.
49. Rana N, Privitera G, Kondolf HC, et al. GSDMB is increased in IBD and regulates epithelial restitution/repair independent of pyroptosis. Cell. 2024;187:1011–5.
50. Odenwald MA, Turner JR. The intestinal epithelial barrier: a therapeutic target? Nat Reviews Gastroenterol Hepatol. 2016;14:9–21.
51. Shi JJ, Zhao Y, Wang K, et al. Cleavage of GSDMD by inflammatory caspases determines pyroptotic cell death. Nature. 2015;526:660–5.
52. Biton M, Haber AL, Rogel N, et al. T helper cell cytokines modulate intestinal stem cell renewal and differentiation. Cell. 2018;175:1307–20.
53. Wan Y, Zhang BK. The impact of zinc and zinc homeostasis on the intestinal mucosal barrier and intestinal diseases. Biomolecules. 2022;12(7):900.
54. Zackular JP, Moore JL, Jordan AT, et al. Dietary zinc alters the microbiota and decreases resistance to Clostridium difficile infection. Nat Med. 2016;22:1330–4.
55. Malamud M, Whitehead L, McIntosh A, et al. Recognition and control of neutrophil extracellular trap formation by MICL. Nature. 2024;633:442–50.
56. Wang L, Xie H, Xu L, et al. rSj16 protects against DSS-Induced colitis by inhibiting the PPAR-α signaling pathway. Theranostics. 2017;7:3446–60.

57. Wang LF, Liao Y, Yang RB, et al. Sja-miR-71a in egg-derived extracellular vesicles suppresses liver fibrosis caused by schistosomiasis via targeting semaphorin 4D. J Extracell Vesicles. 2020;9(1):17857389.

Publisher's note